Fourier Transform Microwave Spectrum and ab Initio Study of Dimethyl Methylphosphonate

ARTICLE *in* JOURNAL OF MOLECULAR SPECTROSCOPY · AUGUST 2001

Impact Factor: 1.48 · DOI: 10.1006/jmsp.2001.8486

Journal of Molecular Spectroscopy **211,** 110–118 (2002)
doi:10.1006/jmsp.2001.8486, available online at http://www.idealibrary.com on IDEAL®

Fourier Transform Microwave Spectrum and *ab Initio* Study of Dimethyl Methylphosphonate

R. D. Suenram,* F. J. Lovas,* D. F. Plusquellic,* A. Lesarri,† Y. Kawashima,‡ J. O. Jensen,§ and A. C. Samuels§

Optical Technology Division, National Institute of Standards and Technology, Gaithersburg, Maryland 20899-8441; †Departamento de Quimica Fisica, Facultad de Ciencias, Universidad de Valladolid, 47005 Valladolid, Spain, ‡Department of Applied Chemistry, Kanagawa Institute of Technology, Atsugi, Kanagawa 243-0292, Japan; and §Passive Standoff Detection Group, Edgewood Chemical and Biological Center, Edgewood Area, Aberdeen, Maryland 21010-5424

Received August 6, 2001; in revised form October 26, 2001

The rotational spectrum of dimethyl methylphosphonate (DMMP) has been studied using a pulsed molecular beam Fourier transform microwave spectrometer. The spectrum is complicated by the internal rotation motions of the three methyl tops in the molecule as well as an interconversion motion of the two methoxy groups. Here, we present the microwave spectrum, the *ab initio* calculations, and the assignment of the rigid-rotor A-symmetry state of the molecule. The rotational constants for this state are $A = 2828.753(2)$ MHz, $B = 1972.360(3)$ MHz, and $C = 1614.267(2)$ MHz. In the following paper, a group theoretical analysis is developed for DMMP. The observed conformation of the molecule has no point-group symmetry and all three electric-dipole selection rules are active, with *c*-type transitions being the most intense. *Ab initio* calculations were carried out at both the Hartree–Fock 6-31G* and MP2/6-311G* levels of theory. These calculations indicate that two low-energy conformations are possible separated by energies of less than 170 cm^{-1}. Furthermore, the calculated lowest energy conformer is in agreement with the one observed experimentally. The relative energies of the two low-energy conformers rise from 34 cm^{-1} at the HF level to 170 cm^{-1} at the MP2 level.

1. INTRODUCTION

Dimethyl methylphosphonate (DMMP), CAS#[756-79-6] with structural formula $(CH_3O)_2P(=O)CH_3$, is among the family of organophosphorus compounds of the general formula $(RO)_2P(=O)CH_3$ (R = methyl, ethyl, and isopropyl) that are often used as model compounds in experimental studies of nerve agents. Compared to the common G-agents (such as Sarin and Soman) DMMP is a relatively nontoxic chemical and is often used to test the sensitivity of analytical techniques. Also, in infrared spectroscopy, DMMP exhibits many of the group frequencies associated with the actual agents, making it an ideal compound to use for evaluating infrared methods of nerve agent detection (*1*).

In a recent study we have used Fourier-transform microwave (FTMW) spectroscopy to observe and assign the rotational spectra of the common G-agents, GA (Tabun), GB (Sarin) (*2*), GD (Soman), and GF (cyclohexyl Sarin). However, to permit the sensitivity of FTMW spectroscopy to be compared directly with that at other analytical techniques, we have now undertaken a microwave investigation of the rotational spectra of DMMP, DEMP, and DIMP where the abbreviations correspond to the dimethyl, diethyl, and diisopropyl analogues, respectively.

Studying DMMP not only leads to a better understanding of trends within the *R*-methylphosphonate class of molecules but also is interesting in its own right. This is due to its large size (seven heavy atoms plus hydrogens) and its considerable conformational flexibility. By studying DMMP, we begin to understand how multiple conformations, large-amplitude motions, tunneling effects, nonrigid rotor line assignments, etc., affect the molecular spectrum. These are all important issues to overcome in order to make FTMW spectroscopy a viable, user-friendly technique for analysis of large, multi-functional-group molecules.

The organization of the manuscript is as follows. Section 2 gives experimental details. Section 3 describes our *ab initio* calculations. Section 4 describes the spectral analysis of an asymmetric rotor fit of tunneling–rotational levels belonging to the totally symmetric symmetry species. (The necessary theoretical results for this section are taken from the following paper (*3*).) Section 5 gives an analysis of the highest methyl top barrier and Section 6 presents a discussion of structural considerations.

2. EXPERIMENTAL

The rotational spectrum of DMMP was observed using a pulsed-molecular-beam, Fabry–Perot cavity, Fourier transform microwave (FTMW) spectrometer of a Balle–Flygare design (*4*). The instrument used was the mini-FTMW spectrometer, as described by Suenram *et al*. (*5*).

A sample of DMMP with a stated purity of 97% (*6*), was purchased from Aldrich Chemical Company and was used without further purification. DMMP is a liquid with a vapor pressure of ~130 Pa [~1 Torr] at room temperature. As such, it requires somewhat different handling to entrain it in a carrier gas at a concentration sufficient to record its rotational spectrum. In the past several years, we have been interested in looking at the rotational spectra of a wide variety of organic compounds of this

0022-2852/02 $35.00

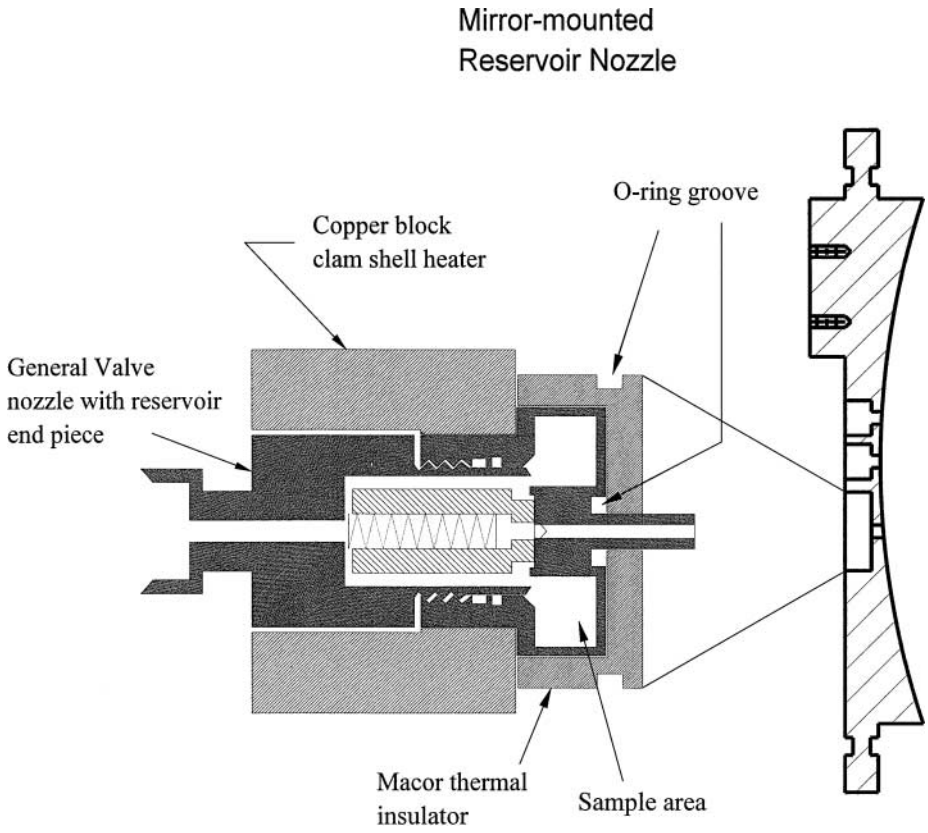

FIG. 1. Heated-reservoir nozzle, showing its location in the end-flange mirror of the mini-FTMW spectrometer.

nature that are either liquids or solids with low vapor pressures at room temperature. To increase the vapor pressure of these compounds to a level sufficient to observe the rotational spectra, we have designed and implemented a heated-reservoir nozzle that is installed in the back side (atmospheric pressure side) of the integral end flange-mirror of the mini-FTMW spectrometer (*5, 7*). This is shown in Fig. 1. For this arrangement, the standard end piece of a high-temperature General Valve Series 9 coil assembly No. 9-279-050-2 (6) has been replaced with an end piece that has a total volume of approximately 1 cm^3. When used in the horizontal orientation, the reservoir can be loaded with 300–400 μl of liquid sample or 300 to 400 mg of solid. Once the nozzle is loaded with a sample and assembled, a clam-shell, copper-block heater is attached to the lower portion of the nozzle (reservoir). Heat is provided by two 2.5 cm $\times$ 0.625 cm diameter "Firerod" heaters (Omega CSH10101100/120) which are rated at 100 W each (*6*). The heater block temperature is monitored via a thermocouple which is inserted into a hole near the bottom of the copper block. To thermally insulate the nozzle from the end flange-mirror, a Teflon or Macor insert is used.

Since the vapor pressure of DMMP is $\sim$130 Pa ($\sim$1 Torr) at room temperature, only mild heating is required to increase the vapor pressure to a sufficient level for observation. Most experiments were carried out with the nozzle temperature between 50 and 100°C. The carrier gas used was and 80%/20% mixture of neon and helium at 150 kPa.

In a set of experiments aimed at determining the minimum detectable signal (smallest concentration of DMMP that can be observed), a number of the stronger transitions could be observed in an eight-component, room-temperature sample mixture which contained only 100 μmole/mole (i.e., 100 ppmv) of DMMP. Furthermore, when using a 1 min average of 600 nozzle pulses, and the carrier gas described above, the minimum detectable signal was determined to be $\sim$2 μmol/mol (i.e., 2 ppmv) at room temperature.

3. *AB INITIO* CALCULATIONS

A search of the DMMP energy surface was carried out using 18 starting geometries involving different orientations of the methoxy groups. Initial searches were carried out at the 6-31G* Hartree–Fock level with zero-point energy corrections included. These calculations converged to four geometries. A second set of higher-level calculations were carried out for these four geometries using Møller–Plessert MP2/6-311++G** theory. In this set of calculations, two of the Hartree–Fock geometries converged to a single point leaving three low-energy forms, referred to as Conformers I, II, and III below. The geometry of the lowest-energy form is shown in Fig. 2. In Table 1 the

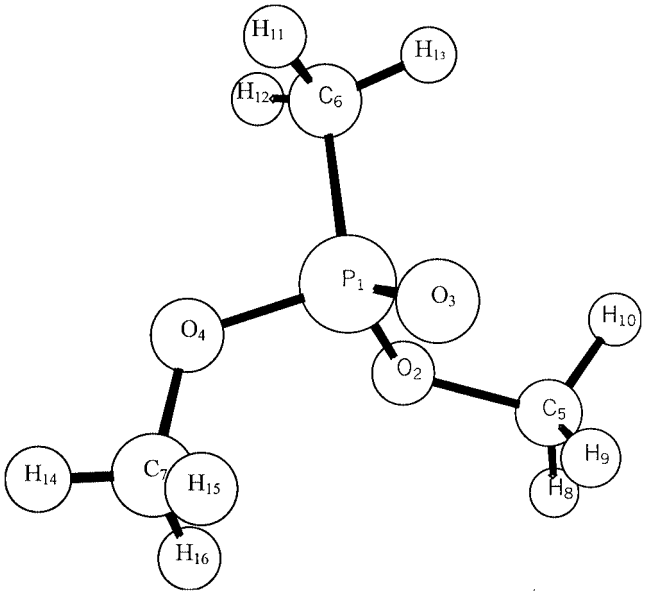

FIG. 2. Calculated lowest-energy conformation of DMMP, based on the present *ab initio* work. The atom numbering is used to designate the different methyl tops.

rotational constants, energies, and electric dipole moment components in the principal axis system are compared with those observed experimentally. Conformers I and II are nearly isoenergetic at both the HF and MP2 levels of theory. Conformer I is has a totally asymmetric geometry with inequivalent methoxy groups, while Conformer II has a plane of symmetry. Conformer III is significantly higher in energy (>600 cm^{-1}) and thus its spectrum would be expected to be much weaker in the 1-K molecular beam, even if the barrier to interconversion were high (*8*). It is interesting that the relative energy of Conformer II is only 34 cm^{-1} at the HF level of theory while it increases to 170 cm^{-1} at the MP2 level. The relative energy of Conformer III, on the other hand, decreases from 937 cm^{-1} to 602 cm^{-1} at the higher MP2 level.

4. SPECTRAL OBSERVATIONS AND ANALYSIS

At the outset, we anticipated that the rotational spectrum of DMMP would be complicated not only by the possibility of the presence of multiple conformations in the gas phase, but also by rather facile internal rotation of the two methoxy methyl tops in the molecule. As described in Section 3 above, high-level *ab initio* calculations were used to gain insight into the number of low-energy conformers expected, as well as the relative magnitude of the internal rotation splittings. These calculations indicated that there could be as many as four possible low-energy conformations in the gas phase sample. For the lowest energy conformation (Fig. 2), the two methoxy methyl tops are inequivalent with rather low barriers ($\leq$400 cm^{-1}) to internal rotation that would cause sizable splittings of the rotational transitions. Conversely, the third methyl top (attached directly to the phosphorus atom) has a high barrier ($\geq$800 cm^{-1}) and would only give rise to very small additional splittings, if any at all. Because of the expected uncertainties associated with the molecular Hamiltonian, it was desirable to record a broad region of the spectral region available. Initially this was accomplished by recording 1-GHz segments of the spectrum and then adding these together using the spectral fitting program developed by Plusquellic (*9*). With the automated scanning features of the software that controls the FTMW instrument (*5*), it takes 1.5 h to record 1 GHz of spectrum using 10 nozzle pulses/step (at a 10-Hz repetition rate) and 500 kHz/step. Accordingly, the region

TABLE 1
Comparison of Theoretical and Experimental Parameters of DMMP

	Energy (cm^{-1})	A (MHz)	B (MHz)	C (MHz)	Δ (uA^2)	μ_a	μ_b	μ_c
Experiment		2828.753(1)[a]	1972.359(1)	1614.268(1)	−121.818		$\mu_c \gg \mu_b \geq \mu_a$	
Conformer I[b]								
HF + ZPE[e]	0	2787(1.48)[c]	1976(−0.19)	1602(0.76)	−122	1.8 [0.54][d]	2.2 [0.65]	7.4 [2.22]
MP2 + ZPE	0	2753(2.68)	1967(0.27)	1612(0.14)	−127			
Conformer II								
HF + ZPE	34	2574(9.01)[c]	2122(−7.59)	1606(−0.51)	−120	4.9 [1.48]	5.5 [1.64]	0 [0]
MP2 + ZPE	170	2534(10.42)	2118(−7.39)	1610(−0.26)	−124			
Conformer III								
HF + ZPE	937	2597(8.19)[c]	2108(−6.88)	1662(−2.96)	−130	4.8 [1.45]	9.1 [2.74]	11.7 [3.51]
MP2 + ZPE	602	2567(9.25)	2112(−7.08)	1672(−3.58)	−134			

[a] Type *A* uncertainties are given with a coverage factor of $k = 1$ (i.e., 1σ).

[b] For Conformer I, the three barriers to internal rotation for the methyl tops were calculated at the HF + ZPE level of theory to be V_3 (Bond 2–5) = 3.36 kJ/mol [281 cm^{-1}]; V_3 (Bond 4–7) = 5.10 kJ/mol [426 cm^{-1}]; V_3 (Bond 1–6) = 9.60 kJ/mol [803 cm^{-1}].

[c] The numbers shown in parentheses are the experimental − theoretical values in percent.

[d] The dipole moment values are given in C·m $\times$ 10^{-30} and [Debye].

[e] Hartree–Fock calculations were carried out at the 6-31G* level while the Møller–Plessert calculations were carried out at the MP2/6-311 + +G** level of theory.

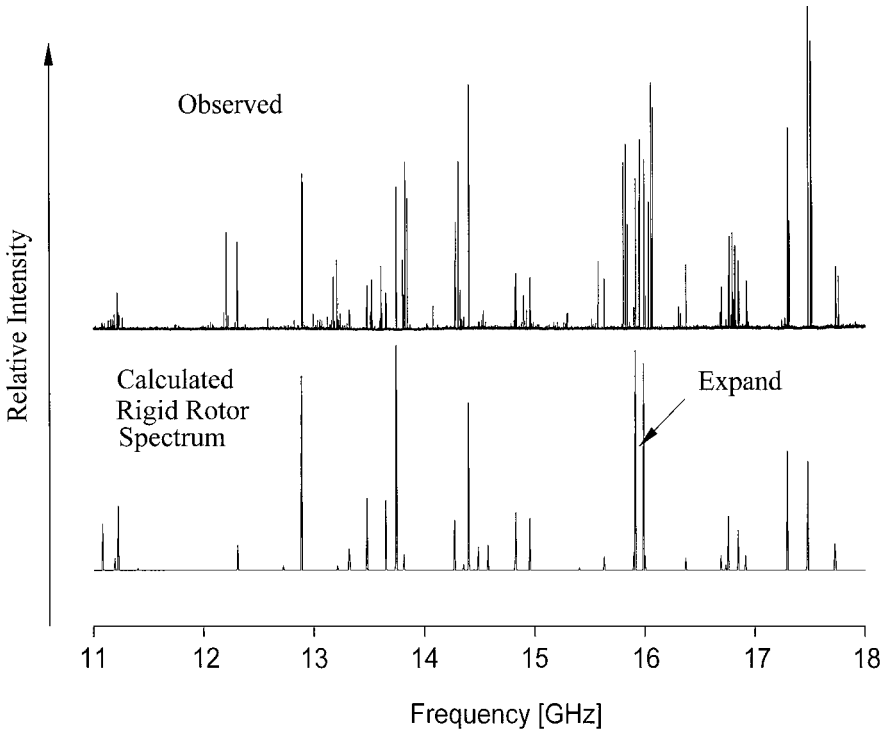

FIG. 3. The 11- to 18-GHz portion of the survey spectrum of DMMP. The top trace shows the observed experimental spectrum and the bottom trace shows the calculated rigid rotor spectrum based on a fit of the A-state transitions.

from 10 to 21 GHz was surveyed. The 11- to 18-GHz portion of this survey scan is shown in the upper trace of Fig. 3. In some of the later work, an additional feature of the instrument control software was introduced that permits unlimited frequency scans to be recorded. With this feature, once a scan is initiated, the instrument automatically scans until the motorized stage controlling the movable mirror, reaches a preset software limit. Once this limit is reached, the mirror is automatically repositioned (backed up) until the next cavity mode is found and the scan is resumed. With this arrangement it is possible to start a scan in the evening and let it run overnight; thus 10 GHz can be surveyed in approximately 15 h using the conditions previously mentioned (*5*).

As a starting point, it is worthwhile to summarize spectral expectations. Structurally, DMMP is expected to have a shape that is more spherical-top in nature than linear. Consequently, we should not expect to see the distinctive *a*-type, *R*-branch pattern of a prolate rotor which many molecular species exhibit. Also, from symmetry considerations we expect that there should be at least two active dipole moment components. The two low-energy conformers predicted by the *ab initio* results are expected to have dominant *c*-type spectra with weaker *b*-type transitions. If there is no symmetry in the molecule (Conformer I), weak *a*-type transitions should also be present. It has been our experience that for spectra of this type, there should be a series of distinctive "quartets" somewhere in the surveyed spectral region. Typically these consist of a pair of *c*-type transitions that are flanked by a pair of *b*-type transitions (or vice versa depending on the rotational constants). If these quartets can be located, they provide a convenient starting point for the spectral assignment. Of course in this case, it may be difficult to locate the quartets if there are additional splittings induced by the internal rotation of the methyl tops.

Once the spectrum had been surveyed, it was a straightforward task to compare the observed spectrum with the spectral predictions generated from the *ab initio* studies. In particular, the *ab initio* generated rotational constants of Conformer I appeared to reproduce the overall features of the observed spectrum, with clumps (or pileups) of transitions approximately where the rotational constants of Conformer I predict a rotational transition. In particular, an interesting cluster of transitions in the vicinity of 16 GHz matched up with one of the aforementioned quartets. This is shown in Fig. 4. This quartet consists of the two strong *c*-type transitions, the 3_{30}–2_{20} and the 3_{31}–2_{21}, flanked by the two weaker *b*-type transitions, the 3_{31}–2_{20} and the 3_{30}–2_{21}. The *b*-type transitions are approximately five times weaker than the strong *c*-type transitions.

As can be seen in the figure, however, the spectral pattern was still confusing, since in addition to the expected quartet, a number of other transitions occurred within ±100 MHz of the chosen lines. Extra transitions were expected, of course, because of internal-rotor splittings induced by the methyl tops. In any case, one anticipates that there would be at least one set of rotational transitions that exhibit nearly rigid-rotor behavior.

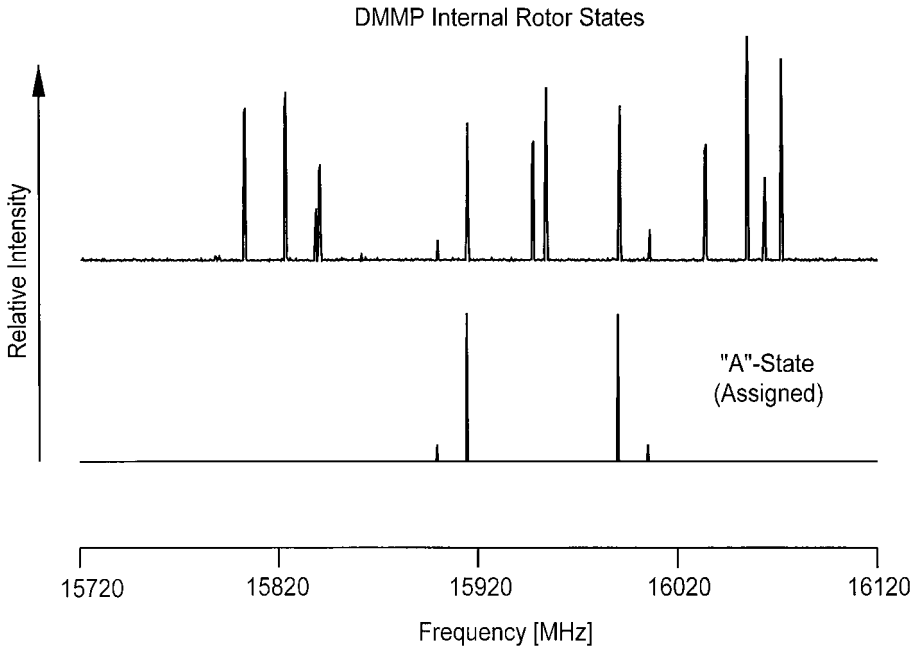

FIG. 4. DMMP spectrum in the region of 16 GHz. Note the highlighted quartet consisting of the two strong *c*-type transitions, the 3_{30}–2_{20} and the 3_{31}–2_{21}, flanked by the two weaker *b*-type transitions, the 3_{31}–2_{20} and the 3_{30}–2_{21}. This quartet was the key to the initial spectral assignment.

This is the "A" state with respect to all internal rotor motions. Indeed, after the JB95 spectral fitting program (*9*) was used to vary the rotational constants to obtain a rather close match of the observed and predicted spectra, additional quartets were located with center frequencies near 10.3 and 21.6 GHz. These are the corresponding 2–1 and 4–3 quartets. Quantum-number assignments permitted a good rigid-rotor fit to be obtained for the *c*- and *b*-type transitions.

Several iterations of adding additional transitions to the first group assigned, followed by refitting, led to a set of 14 *b*- and *c*-type transitions that could be fit reasonably well using a standard rigid-rotor Hamiltonian. From these fits, *a*-type transitions were predicted. Although there were transitions in the general vicinity of all of the predicted *a*-type lines, they could not be fit together with the *b*- and *c*-types. Figure 5 shows a high-resolution scan near 13.5 GHz where the 4_{14}–3_{13} and the 4_{04}–3_{03} *a*-type pair is predicted. The two arrows at the bottom show the exact location of the two transitions as predicted from the *b*- and *c*-type fit. As it turned out, in addition to the internal rotation splittings of the methoxy methyl tops, there is a tunneling splitting in which the inequivalent methoxy tops exchange conformational orientations in the molecule. If one averages the frequencies of the two transition pairs as shown by the arrows in the upper part of the figure, the corresponding *a*-type transition frequencies can be used in the fit along with the *b*- and *c*-type transitions. In fact, for most of the *b*- and *c*-type transitions used in the rigid rotor fits, an averaged center frequency was actually also used since many of the transitions consisted of partially resolved multiplets. (The small splitting in the *b*- and *c*-type transitions correspond to bottom–bottom and top–top selection rules with respect to the methoxy interchange motion, whereas the large splittings in the *a*-type transitions correspond to bottom–top and top–bottom selection rules.) Thirty asymmetric-rotor-like transitions are listed in Table 2 along with the observed minus calculated values. The standard deviation of the fit is 5 kHz, which is fairly good considering that the average frequency of a number of widely split doublets (for the a-type transitions) were used in the fits and that the estimated uncertainty in the individual measurements is approximately 6 to 10 kHz. The resulting rotational constants and distortion parameters are listed in Table 3.

It is interesting to note that the eight observed transitions shown in Fig. 5 for the 4_{14}–3_{13} and 4_{04}–3_{03} *a*-type transitions display rather characteristic relative intensity patterns. Qualitatively these patterns have relative intensities that approximate 2 : 4 : 2 : 1 : 1 : 4 : 1 : 1 and 1 : 1 : 4 : 1 : 1 : 2 : 4 : 2, respectively, where the transitions with intensity 2 correspond to those used in the asymmetric rotor fit. The *b*- and *c*-type transitions, however, do not appear to exhibit this or any other obvious characteristic intensity pattern. The *a*-type pattern can be understood using group theory as described in detail in the companion paper (*3*). The physical ideas used as input and the group-theoretical conclusions obtained as output can be briefly summarized as follows. Based on the Hartree–Fock *ab initio* calculation we expect the various large-amplitude motions in this molecule to consist of three methyl-top internal rotations (with a low, medium, and high barrier, respectively) together with a concerted internal rotation about both P–O bonds which interchanges the role of the inequivalent methoxy groups in the molecule. The smallest splittings are expected to arise from the highest methyl top barrier associated with the methyl group attached directly to the

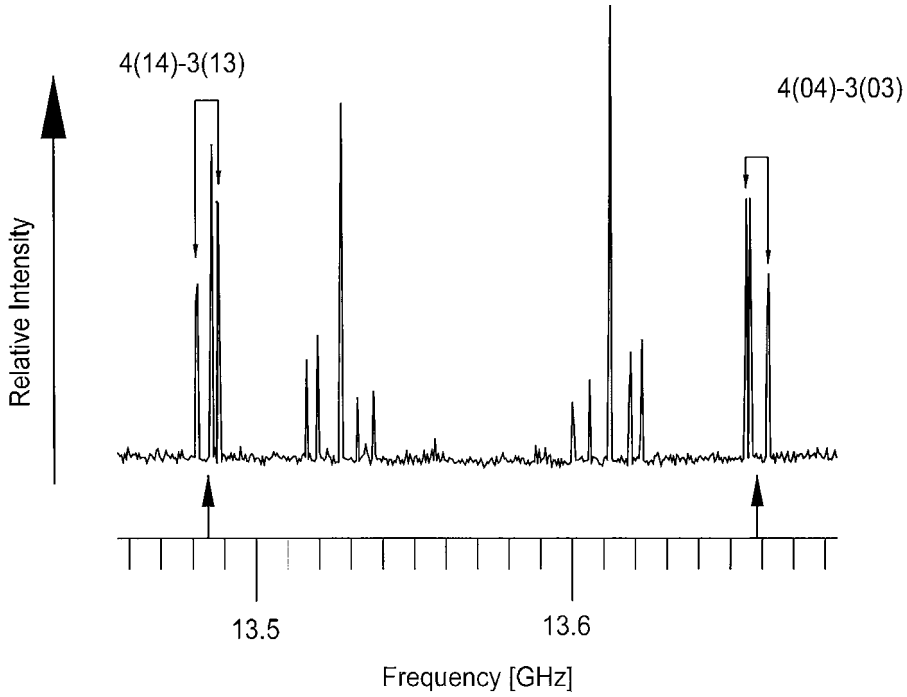

FIG. 5. Spectral lines in the region of the 4_{14}–3_{13} and 4_{04}–3_{03} transitions of DMMP. Note the pattern of two strong lines, two medium lines, and four weak lines, corresponding closely to the theoretically expected (*3*) tunneling component symmetry species and statistical weights (in parentheses) of $A_1(2) + A_2(2) + 2E(1) + E_{1sep}(1) + E_{2sep}(1) + 2G_{sep}(4)$.

phosphorus atom. These splittings are only slightly larger than the instrumental resolution and generally give rise to complicated, but only partially resolved, lineshapes. The largest splittings presumably arise from the lowest methyl top barrier which by itself would split each asymmetric rotor level into one A_{1top} and one E_{1top} component, where the subscript "1top" is used to indicate the well-known A/E torsional component in a molecule with one methyl rotor. In DMMP, this A_{1top} component is further split by the medium-barrier methyl top internal rotation and the methoxy interchange motion, which are of comparable magnitude, into a three-level pattern with relative statistical weights 2 : 4 : 2. The E_{1top} component is correspondingly split into a five-level pattern with weights 1 : 1 : 2 : 1 : 1. In the full permutation inversion group G_{18} for DMMP, these levels have species A_1, G_{sep}, A_2 and E_{1sep}, E_{2sep}, G_{sep}, E, E, (see Fig. 2 of Ref. 3) indicating that the original 1 : 2 degeneracy ratio for the one-top A_{1top}:E_{1top} pattern is preserved. (Note, however, that the ordering in frequency space of transitions involving these split levels can be different).

One of the experimental observations used to aid in the assignment or classification of the observed transitions is their lineshape. The lineshapes of the individual transitions vary because of smaller splittings induced by internal rotation of the third methyl top (the one attached directly to the phosphorus atom) (*3*). This is discussed in detail in (*3*), where group theoretical methods are developed for the G_{54} group. The G_{54} group is necessary to completely describe all the splittings that arise when three methyl top torsions, plus the methoxy top exchange, are present in the molecule. These characteristic lineshapes are particularly evident for the *a*-type transitions, which suffer less from overlapping and blending than the *b*- and *c*-type transitions. Figure 6 shows representative lineshapes for transitions with G_{18} symmetry species. At low J, many transitions for the A_1 and A_2 states are observed as singlets (6a), while some are split due to interactions with the internal rotation of the high-barrier P–CH_3 top. These interactions cause a doublet splitting into equal intensity components to become large enough to be observable (6b). This is also true for E state transitions (6c). Transitions associated with the E_{1sep}, E_{2sep}, and G_{sep} states typically are split into partially resolved triplets, whose components exhibit a 1 : 2 : 1 intensity pattern (6d and 6e). Figure 6f illustrates what we believe is a *c*-type transition with four nearly equal components that we assume represents two nearly overlapping doublet transitions. Intensity and pump-pulse characteristics lead us to a G_{sep}-state inference; however, the fact that the transition appears to consist of two doublets would be more indicative of an E, E_{1sep}, or E_{2sep} state. Hopefully this question will be resolved once all the spectral splittings are better understood.

The lineshapes shown in Fig. 6 are relatively reproducible from one J to the next and thus permit one to deduce the proper transition when the region of interest is spectrally cluttered. Once the transitions have been chosen, identities can be confirmed by using combination-difference frequency loops. This is described in further detail in (*3*).

TABLE 2
Rigid Rotor Fit of Selected "*A*"-State Rotational Transitions of DMMP

Transition	Frequency (MHz)[a]	Obs. - Calc. (kHz)
3_{03}–2_{12}	9839.9854	0.4
2_{21}–1_{10}	10100.4688	0.7
2_{20}–1_{10}	10191.3516	1.7
3_{03}–2_{02}	10429.1973[b]	−1.8
2_{21}–1_{11}	10458.5577	−1.4
2_{20}–1_{11}	10549.4414	3.3
3_{22}–2_{21}	10759.8660[b]	−0.7
3_{13}–2_{02}	10760.8174	1.0
3_{21}–2_{20}	11090.4463	3.2
4_{04}–3_{13}	13326.7281	−9.6
3_{22}–2_{11}	13329.0142	−4.6
4_{14}–3_{13}	13484.7137[b]	7.4
4_{04}–3_{03}	13658.3462[b]	−8.8
3_{21}–2_{11}	13750.4746	−2.4
4_{14}–3_{03}	13816.3340	10.3
3_{21}–2_{12}	14824.7154	−6.5
4_{13}–3_{12}	14831.0994[b]	2.7
3_{31}–2_{20}	15897.0273	−0.6
3_{30}–2_{20}	15912.0147	0.8
3_{31}–2_{21}	15987.9092	−0.5
3_{30}–2_{21}	16002.8975	1.8
5_{15}–4_{14}	16761.6031[b]	27.2[c]
5_{05}–4_{04}	16852.3145[b]	−26.3[c]
4_{13}–3_{03}	17296.1636	4.8
4_{22}–3_{12}	17480.1028	−1.6
5_{14}–4_{13}	18281.1260[b]	−1.0
4_{41}–3_{30}	21599.5635	0.5
4_{40}–3_{30}	21601.6016	1.6
4_{41}–3_{31}	21614.5445	−4.5
4_{40}–3_{31}	21616.5884	2.4

[a] The frequencies of these transitions, which involve rotational levels of the totally symmetric "A" state with respect to all internal rotor motions, are given in MHz. The combined standard uncertainties (i.e., $k = 1$ or 1σ) of the frequency measurements are 10 kHz.

[b] For the *a*-type transitions, the values here are the average frequency of pairs of lines split by several MHz.

[c] Not fit.

TABLE 3
Rotational Constants for the "*A*"-State of DMMP Derived from the Transitions in Table 2

Parameter[a]	Value
A (MHz)	2828.7527(8)
B (MHz)	1972.3591(8)
C (MHz)	1614.2676(10)
Δ_{JK} (kHz)	−3.80(14)
Δ_J (kHz)	0.97(2)
Δ_K (kHz)	7.46(15)
δ_J (kHz)	0.41(2)
δ_K (kHz)	fixed at 0

[a] Type *A* uncertainties are given with a coverage factor $k = 1$, i.e., 1 std. dev.

Figure 2 of Ref. (*3*) presents the sequence of tunneling splittings obtained when the P–CH_3 (third top) internal rotation is frozen and the other motions are turned on in the order low-barrier top, medium-barrier top, top–top interaction, and methoxy interchange. As explained summarily above and in more detail in Ref. (*3*), one expects each asymmetric rotor transition to split into eight components, with G_{18} group theoretical species (and statistical weights) given by $A_1(2) + A_2(2) + 2E(1) + E_{1sep}(1) + E_{2sep}(1) + 2G_{sep}(4)$. One further expects an $A_1(2) + A_2(2) + G_{sep}(4)$ pattern arising from further splittings of the A_{1top} component of the dominant internal rotation splitting and a $2E(1) + E_{1sep}(1) + E_{2sep}(1) + G_{sep}(4)$ pattern arising from further splittings of the E_{1top} component of the dominant internal rotation splitting.

5. V_3 BARRIER FOR THE HIGH-BARRIER P–CH_3 TOP

The A–E internal rotation splittings caused by the CH_3–P methyl group were partially resolved on eight of the transitions in Table 2. While it is beyond the scope of this paper to fit the low-barrier internal rotation splittings of the methoxy tops, we can use standard one-top IAM theory (10) to estimate the barrier to internal rotation of the high-barrier CH_3–P top. To do this, the splitting pattern was initially simulated with the *ab initio* parameters using $\theta = 78^\circ$ (C–P bond angle to the *a*-axis) and $V_3 = 803$ cm^{-1} and the IAM treatment with a program written by Bauder and Guenthard (*11*). Table 4 lists eight one-top A, E pairs of transitions which were fit along with the remaining other 22 transitions in Table 2. The rotational constants and centrifugal distortion parameters used were essentially the same as given in Table 3. The methyl top moment of inertia, I_α, was fixed at a value of 3.2 uÅ^2 and in the fit, values for the internal rotation parameters θ and V_3 were determined to be $\theta = 84.5(14)^\circ$ and $V_3 = 662(6)$ cm^{-1}. These are in fair agreement with the theoretical values quoted above. An improved analysis will require higher-resolution measurements and analysis of blended components.

6. STRUCTURAL CONSIDERATIONS

Comparing the *ab initio*-calculated parameters for conformers I and II with the experimental data in Table 1 leads to the conclusion that the conformer that best models the experimental results is Conformer I. The experiment–theory residuals for the rotational constants and the inertial defect of Conformer I are quite small, on the order of 1% to 2% for *A* and <1% for *B* and *C*. The relative ordering of the electric dipole moment component magnitudes also agrees for Conformer I and clearly indicates that the observed conformer has a totally asymmetric structure. It is interesting that the lower-level Hartree–Fock calculations approximate the rotational constants and inertial defect more closely than the higher-level MP2 calculations. The relative energies of all three conformers vary somewhat depending on the level of theory used, but the difference in energy between

TABLE 4
Internal Rotation Splittings of the "*A*"-State Transitions Caused by the High-Barrier P–CH_3 Top

Transition	ν_A (MHz)	Obs - Calc (kHz)	ν_E (MHz)	Obs - Calc (kHz)
3_{03}–2_{12}	9839.992	1	9839.979	4
3_{21}–2_{20}	11090.460	6	11090.435	9
4_{04}–3_{13}	13326.734	−10	13326.722	−7
3_{21}–2_{12}	14824.730	−3	14824.701	0
4_{13}–3_{03}	17296.195	14	17296.131	2
4_{22}–3_{12}	17480.113	−2	17480.092	4
5_{14}–4_{13}	18281.135	−10	18281.117	−4

$I_\alpha = 3.2$ uÅ^2 (fixed)
$\theta = 84.5(14)^{\circ a}$
$V_3 = 662\ (6)$ cm^{-1}

[a] Type *A* uncertainties are given with a coverage factor $k = 1$, i.e., 1 std. dev.

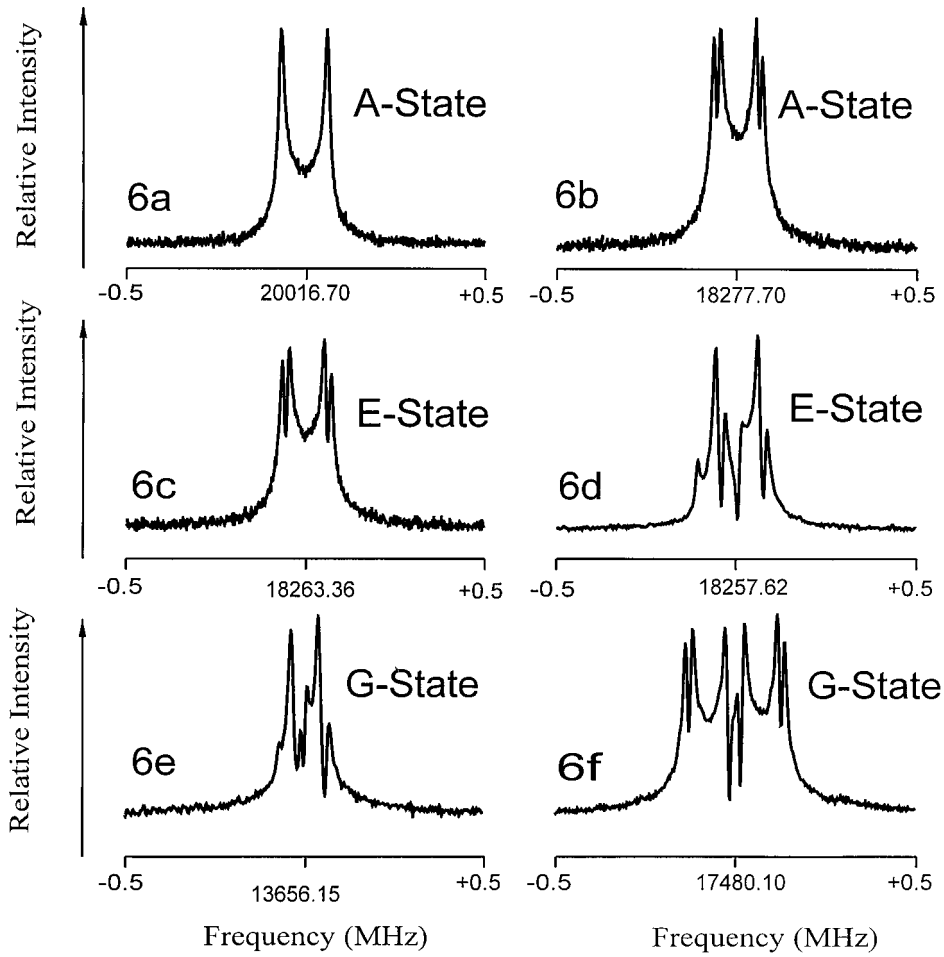

FIG. 6. High-resolution traces for selected *a*-type transitions similar to the ones shown in Fig. 5. The doubling into two distinct sets of partially resolved components arises from the Doppler effect resulting from the coaxial arrangement of the molecular beam with the axis of the microwave cavity. Note the splitting of these transitions into two, three, and four partially resolved components, corresponding to the expected theoretically predicted (*3*) patterns when the smallest tunneling splitting, arising from the high-barrier internal rotation of the P–CH_3 top, is turned on.

TABLE 5
Conformer I Atomic Coordinates[a] in the Principal Axis System from the Hartree–Fock *ab Initio* Calculations

Atom	A	B	C
P(1)	0.00042	0.358852	0.133742
O(2)	0.937673	−0.646138	−0.673217
O(3)	0.145006	0.241719	1.579679
O(4)	−1.430217	0.03101	−0.454821
C(5)	2.14098	−1.156119	−0.122
C(6)	0.312347	1.98375	−0.562528
C(7)	−2.122123	−1.152331	−0.086269
H(8)	2.451389	−1.970081	−0.759282
H(9)	1.979563	−1.50883	0.885121
H(10)	2.908164	−0.391538	−0.119078
H(11)	−0.378237	2.699664	−0.134109
H(12)	0.189951	1.968058	−1.638
H(13)	1.322954	2.292743	−0.321631
H(14)	−3.105612	−1.083775	−0.524443
H(15)	−2.200403	−1.222448	0.989275
H(16)	−1.608559	−2.020083	−0.478301

[a] The coordinates are given to six figures in order that bond lengths and angles can be calculated without roundoff errors.

Conformers I and II is so small that they are essentially degenerate within the margin of uncertainty for this type of calculation.

The atomic coordinates for Conformer I from the Hartree–Fock level of theory are shown in Table 5. The atom numbering corresponds to that shown in Fig. 2. The coordinates, while not accurate to the six digits that are given, are expressed in this fashion in order to allow bond lengths and angles to be calculated from the coordinates. Since isotopic substitutions have not been made we cannot directly compare the theoretical and experimental structures. However, we can make an indirect comparison of the theoretical results with experiment by looking at the calculated and observed rotational constants. Table 3 indicates that A, B, and C from the asymmetric rotor fit of the hypothetical center frequencies in Table 2 are within $\lesssim$2% of the *ab initio* values calculated for Conformer I shown in Table 1. Quantitative comparison of the experimental and *ab initio* barrier heights is not possible at the moment, since a more complete global fit of the splitting patterns will be necessary before the contributions from the individual tunneling motions can be untangled from each other. Nevertheless, the qualitative *ab initio* division of the three barriers into low, medium, and high is clearly correct.

There is significant interest in the catalytic activity and decomposition mechanisms of DMMP on a number of different catalytic surfaces (*12–15*). Now that the conformational geometry of DMMP and the relative magnitudes of the dipole moment components are known, this information could be useful in aiding the understanding of the catalytic interactions and decomposition mechanisms of DMMP on these surfaces.

The most interesting structural parameters are the values of the torsional angles about the two P−O bonds. These are of interest from the point of view of analogous studies involving protein folding via rotation about single bonds in biomimetic molecules. These two angles should be obtainable from substitution structures for the two isotopomers corresponding to each methoxy methyl carbon in turn being replaced by ^{13}C. The present signal to noise indicates that with some effort, the two C−O−P=O dihedral angles might be determinable from a sample with natural isotopic abundances.

Finally, from an analytical chemistry standpoint, it is desirable to fully understand the methyl-top splittings and the full group theoretical behavior since, as indicated above, the *c*-type (dominant dipole moment component) G_{sep}-state transitions should be the most intense in the entire spectrum because they have a statistical weight that is a factor of 2 larger than the comparable A_1- and A_2-state transitions and a factor of 4 stronger than the E, E_{1sep}, or E_{2sep} state transitions. Thus if one should use G_{sep}-state transitions as an analytical feature when using FTMW spectroscopy for monitoring for the presence of DMMP in sample mixtures, the detection limit should, in principle, be a factor of 2 lower than if A_1- or A_2-state transitions were used. Unfortunately, at this point of the work, only the A_1- and A_2-state transitions are fully understood.

ACKNOWLEDGMENTS

The authors are deeply indebted to Jon Hougen, who recognized that there was an internal conversion of the methoxy tops within the molecule, which explained why the individual *a*-type transitions could not be fit along with the *b*- and *c*-types, and who offered numerous helpful suggestions during the course of the preparation of the manuscript. The authors gratefully acknowledge partial financial support from the Defense Threat Reduction Agency, Contract 003422. A. L. gratefully acknowledges a DGES grant to visit the NIST.

REFERENCES

1. L. Bertilsson, D. Potje-Kamloth, H. D. Liess, I. Enquist, and B. Liedberg, *J. Phys. Chem. B*. **102,** 1260–1269 (1998).
2. A. R. Hight Walker, R. D. Suenram, A. C. Samuels, J. O. Jensen, M. W. Ellzy, J. M. Lochner, and D. Zeroka, *J. Mol. Spectrosc*, in press (2001).
3. N. Ohashi and J. T. Hougen, *J. Mol. Spectrosc.*,
4. T. J. Balle and W. H. Flygare, *Rev. Sci. Instrum*. **52,** 33–45 (1981).
5. R. D. Suenram, J. U. Grabow, A. Zuban, and I. Leonov, *Rev. Sci. Instrum*. **70,** 2127–2135 (1999).
6. In order to adequately describe certain instrumentation, brand names and model numbers are used. The use of these names does not imply an endorsement by the NIST in any way.
7. S. Davis, D. F. Plusquellic, R. D. Suenram, and R. Lavrich, in preparation.
8. R. S. Rouff, T. D. Klotts, T. Emilsson, and H. S. Gutowsky, *J. Chem. Phys*. **93,** 3142–3150 (1990).
9. D. F. Plusquellic, R. D. Suenram, B. Maté, J. O. Jensen, and A. C. Samuels, *J. Chem. Phys*, in press (2001).
10. R. C. Woods, *J. Mol. Spectrosc*. **21,** 4–24 (1966).
11. A. Bauder and Hs. H. Guenthard, *J. Mol. Spectrosc*. **60,** 290–311 (1976).
12. S. R. Segal, S. L. Suib, X. Tang, and S. Satyapal, *Chem. Mater*. **11,** 1687–1695 (1999).
13. C. N. Rusu and J. T. Yates, Jr., *J. Phys. Chem. B* **104** 12 292–12 298 (2000).
14. C. N. Rusu and J. T. Yates, Jr., *J. Phys. Chem. B* **104** 12 299–12 305 (2000).
15. L. Bertilsson, K. Potje-Kamloth, H. D. Liess, I. Engquist, and B. Liedberg, *J. Phys. Chem. B* **102** 1260–1269 (1998).